nature photonics

LETTERS

https://doi.org/10.1038/s41566-018-0240-2

Experimental demonstration of a three-dimensional lithium niobate nonlinear photonic crystal

Dunzhao Wei[1,4], Chaowei Wang[2,4], Huijun Wang[1,4], Xiaopeng Hu[1,4], Dan Wei[1], Xinyuan Fang[1], Yong Zhang[1*], Dong Wu[2*], Yanlei Hu[2], Jiawen Li[2], Shining Zhu[1*] and Min Xiao[1,3*]

A nonlinear photonic crystal (NPC)[1] possesses space-dependent second-order nonlinear coefficients, which can effectively control nonlinear optical interactions through quasi-phase matching[2]. Lithium niobate ($LiNbO_3$) crystal is one of the most popular materials from which to fabricate NPC structures because of its excellent nonlinear optical properties[3–5]. One- and two-dimensional $LiNbO_3$ NPCs have been widely utilized in laser frequency conversion[6,7], spatial light modulation[8–12] and nonlinear optical imaging[13,14]. However, limited by traditional poling methods, the experimental realization of three-dimensional (3D) NPCs remains one of the greatest challenges in the field of nonlinear optics[1,15]. Here, we present an experimental demonstration of a 3D $LiNbO_3$ NPC by using a femtosecond laser to selectively erase the nonlinear coefficients in a $LiNbO_3$ crystal[16,17]. The effective conversion efficiency is comparable to that of typical quasi-phase-matching processes. Such a 3D $LiNbO_3$ NPC provides a promising platform for future nonlinear optical studies based on its unique ability to control nonlinear interacting waves in 3D configuration.

In nonlinear wave-mixing processes inside nonlinear crystals, phase matching is normally required for high-efficiency frequency conversion[2]. Taking the second-harmonic generation (SHG) process as an example, the amplitude of the generated second-harmonic (SH) field will increase linearly with crystal length if the phase-matching condition is perfectly satisfied (red line in Fig. 1a). However, because of the dispersion-induced phase mismatch, the SH field normally oscillates along the propagation direction with a period of $2l_c$, where l_c is the coherence length of the nonlinear interaction (black line in Fig. 1a)[3]. The quasi-phase-matching (QPM) technique is an effective and popular solution for overcoming such a phase mismatch and enhancing the overall conversion efficiency, which can be fulfilled in an NPC such as an electrically poled $LiNbO_3$ crystal[4,5]. By periodically inverting the sign of the nonlinear coefficient with a period of $2l_c$, the generated SH field can continuously increase along the propagation direction (green line in Fig. 1a). Until now, QPM processes have only been realized in one- and two-dimensional cases because of the limitations in traditional fabrication methods. The concept of a 3D NPC has been proposed for 3D QPM since 1998[1]. In addition, 3D NPCs have unique applications in 3D nonlinear beam shaping[12], 3D nonlinear holography[9] and high-dimensional entanglement[7]. However, the fabrication of 3D NPCs remains a great challenge in the field of nonlinear optics.

The most popular way to fabricate a $LiNbO_3$ NPC structure is to use the electric poling method. In this method, ferroelectric domains in the $LiNbO_3$ crystal are selectively inverted by applying an external electric field[5]. Other methods include chemical indiffusion, scanning force microscopic poling, electron-beam poling, probe-tip poling and the crystal-growing technique, which have been developed for specific circumstances such as periodically poled $LiNbO_3$ waveguides, surface poling and short-pitch poling[18–22]. However, none of the above traditional techniques can be used to fabricate 3D NPC structures.

Laser writing is one of the potentially suitable candidates for accomplishing this milestone because it can efficiently create 3D structures in transparent materials[23,24]. Recently, one- and two-dimensional domain structures have been realized on the surface of $LiNbO_3$ and strontium barium niobate crystals by ultraviolet light poling using the pyroelectric effect[25,26]. Near-infrared femtosecond laser poling through a localized thermo-electric field has also been experimentally demonstrated in a Ti-indiffused $LiNbO_3$ waveguide[27]. However, it remains a great challenge to directly pole the domains inside a nonlinear crystal. Indeed, a 3D-poled $LiNbO_3$ NPC has not yet been demonstrated.

In this Letter, we experimentally demonstrate a different type of 3D $LiNbO_3$ NPC realized through a femtosecond laser engineering method. Instead of trying to pole the ferroelectric domains in a $LiNbO_3$ crystal, we optimize the laser parameters to selectively erase the nonlinear coefficients $\chi^{(2)}$ of the $LiNbO_3$ crystal in a certain pattern[16,17]. The physical mechanism can be understood as one that reduces the crystallinity through laser irradiation, which was verified by measurements of the transmission electron microscopy (TEM) diffraction pattern and micro-Raman signal in the engineered area (see Supplementary Sections 1 and 2 for details). The nonlinear interacting waves in a periodically poled $LiNbO_3$ crystal are phase-modulated by the inverted ferroelectric domains, which, alternatively, are spatially amplitude-modulated in the laser-engineered $LiNbO_3$ crystal. In an ideal case, an amorphous structure forms in the engineered area, which can reduce the nonlinear coefficients to zero. When the nonlinear coefficients are periodically erased, the SH field increases in the first coherence length l_c, remains unchanged in the second, and then repeats this pattern

[1]National Laboratory of Solid State Microstructures, College of Engineering and Applied Sciences, and School of Physics, and Collaborative Innovation Center of Advanced Microstructures, Nanjing University, Nanjing, China. [2]CAS Key Laboratory of Mechanical Behavior and Design of Materials, Department of Precision Machinery and Precision Instrumentation, University of Science and Technology of China, Hefei, China. [3]Department of Physics, University of Arkansas, Fayetteville, AR, USA. [4]These authors contributed equally: Dunzhao Wei, Chaowei Wang, Huijun Wang, Xiaopeng Hu. *e-mail: zhangyong@nju.edu.cn; dongwu@ustc.edu.cn; zhusn@nju.edu.cn; mxiao@uark.edu

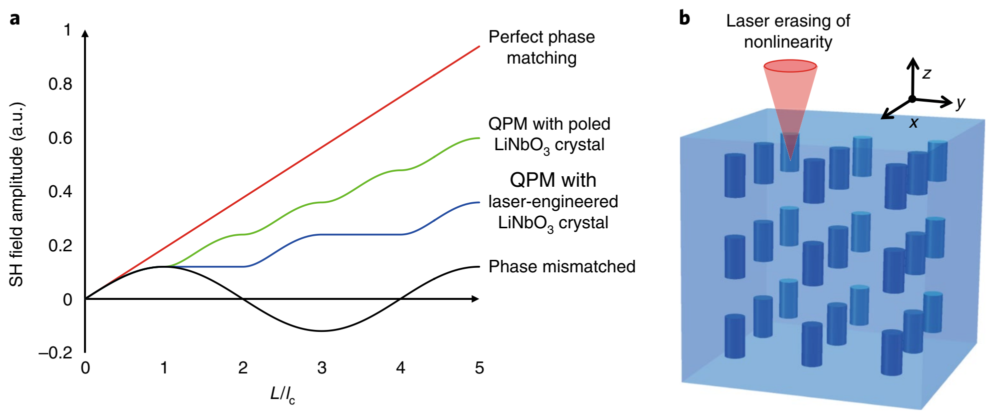

Fig. 1 | QPM mechanism in laser-engineered $LiNbO_3$ crystal. a, The amplitude of the generated SH field strongly depends on the phase-matching mechanism. Generally, the SH field oscillates along the propagation direction because of the phase mismatch (black line). If the mismatch is perfectly compensated, the SH field will increase linearly (red line). Such an ideal case is normally hard to realize in a natural $LiNbO_3$ crystal. QPM provides a powerful solution to achieve efficient SHG by introducing a periodically poled domain structure in a $LiNbO_3$ crystal (green line). If one uses laser-engineered $LiNbO_3$ crystal, the QPM mechanism still works by periodically modulating the amplitudes of the nonlinear coefficients (blue line). Although the conversion efficiency is lower than that for a perfectly poled crystal, it is feasible to realize a 3D NPC structure with such a laser engineering method. **b**, Schematic diagram of the 3D NPC fabrication realized through femtosecond laser engineering.

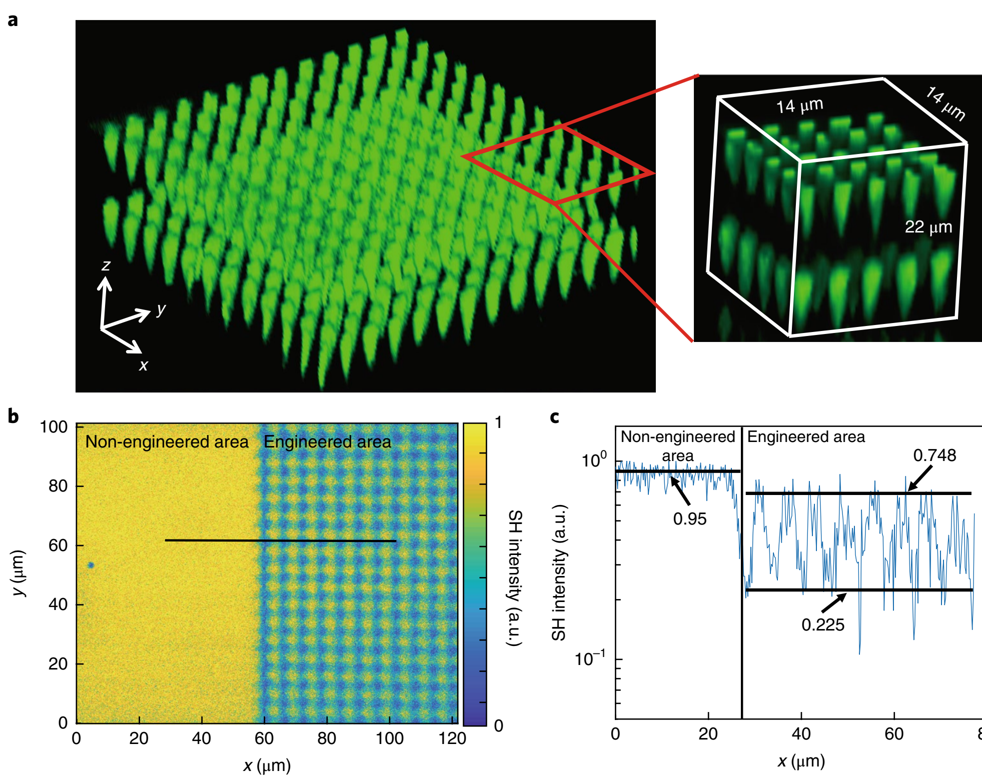

Fig. 2 | Sample characterization. a, Image of the 3D structure recorded using Čerenkov-type SH confocal microscopy[11,28] (see Supplementary Section 9 for details). The recorded image shows the first two layers in the 3D $LiNbO_3$ NPC, which presents a clear periodic structure. **b**, SH image in the *x*–*y* plane through a general confocal SH microscopic system. **c**, Intensity distribution along the black line in **b**. The average values of the SH intensities at various positions are also shown. The SH intensity in the engineered area is much lower than that in the non-engineered area, confirming the greatly reduced nonlinear coefficients due to the laser engineering process. The non-zero minimal SH intensity in **c** indicates that $\chi^{(2)}$ can be further reduced. The difference in maximal SH intensities for engineered and non-engineered areas can be attributed to the slight reduction in $\chi^{(2)}$ caused by the unfocused writing laser beam and scattering loss in the 3D structure.

of increasing energy flux (blue line in Fig. 1a). Although the theoretical conversion efficiency in a laser-engineered $LiNbO_3$ crystal is one-quarter that in an ideal electrically poled nonlinear crystal (see Supplementary Section 6.1 for calculations), it is still significantly enhanced compared to that in the phase-mismatched case (Fig. 1a). The requirements for this laser engineering (especially along the depth direction) are much easier to satisfy than those for the laser poling method. More importantly, this technique can be used to

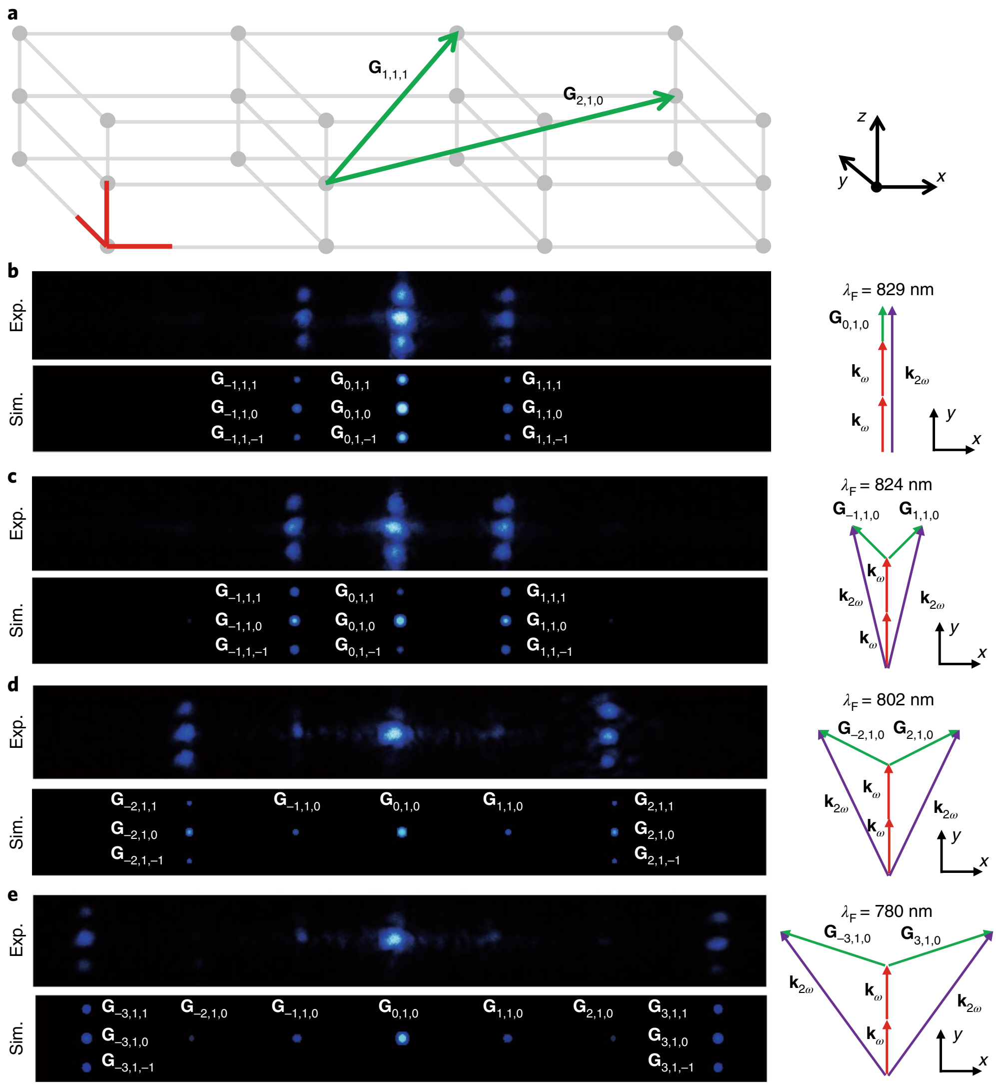

Fig. 3 | Demonstration of SHG processes in a 3D $LiNbO_3$ NPC. a, 3D reciprocal lattice and typical 3D reciprocal vectors. Red lines in **a** represent unit lengths (defined by $2\pi/\Lambda_z$) along the *x*, *y* and *z* axes. **b**–**e**, Measured (Exp.) and simulated (Sim.) 3D QPM SH beam patterns at various input fundamental wavelengths. The QPM configurations, as well as the corresponding reciprocal vectors, are presented in the right column. Note that not all SH spots in **b**–**e** are perfectly phase-matched (see Supplementary Sections 5, 6 and 7 for details).

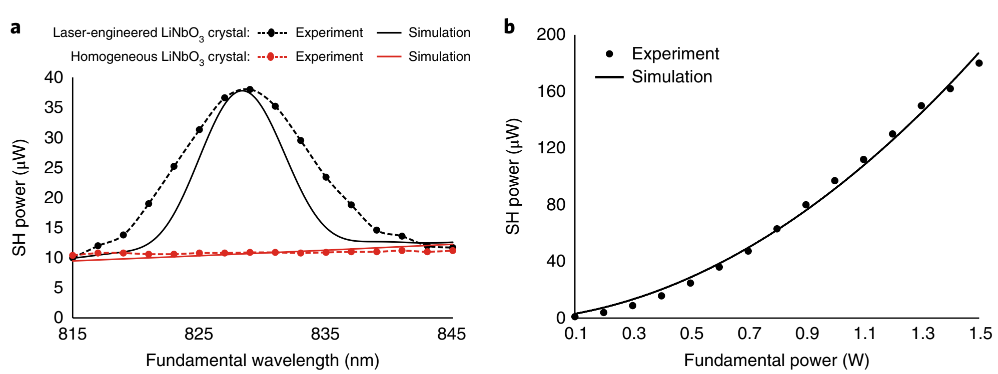

Fig. 4 | Measured dependences of SH power on input parameters. a, Dependence of SH power on fundamental wavelength. The peak at 829 nm (black curve) results from the QPM SHG process assisted by the reciprocal vector $G_{0,1,0}$, which is greatly enhanced in comparison to the non-QPM case (red curve). The simulated curves (calculated from Supplementary equation 14 in Supplementary Section 6.2) agree well with the experimental results. **b**, Corresponding dependence of QPM SH power on input pump power at the fundamental wavelength of 829 nm. The relationship agrees well with a quadratic curve. At a pump power of 1.5 W, the output SH power reaches ~180 μW.

fabricate arbitrary 3D NPC structures (Fig. 1b) in most nonlinear materials, including $LiNbO_3$ crystals.

We designed a 3D NPC with a tetragonally engineered structure, as shown in Fig. 1b. The structural unit was chosen to be a cylinder to simplify the laser engineering process in the direction of the depth (z axis). In the experiment, we fabricated the 3D NPC structure in a z-cut 5% MgO-doped $LiNbO_3$ crystal using a femtosecond laser engineering technique (see Methods and Supplementary Section 4 for the laser engineering process). The periods are $\Lambda_x = 3\,\mu m$, $\Lambda_y = 3\,\mu m$ and $\Lambda_z = 11\,\mu m$. Figure 2a shows a Čerenkov-type SH confocal microscopic image of the sample[28]. The engineered areas present a well-defined periodic structure, as designed. Laser engineering of the nonlinear coefficients in the $LiNbO_3$ crystal was characterized by general confocal SH microscopy. The recorded SH intensities in the x–y plane for the engineered and non-engineered regions are shown in Fig. 2b,c. Clearly, the SH signals in the centres of the engineered spots are much weaker than the signal from the non-engineered area, which indicates greatly reduced nonlinear coefficients due to the laser erasing process.

Next, we performed SHG experiments to demonstrate the 3D QPM processes in the 3D $LiNbO_3$ NPC (see Methods and Supplementary Section 8 for the experimental scheme). Figure 3 depicts the reciprocal lattice and typical 3D QPM SHG configurations. The 3D QPM conditions can be written as

$$\mathbf{k}_{2\omega} - 2\mathbf{k}_{\omega} - \mathbf{G}_{m,n,l} = 0 \quad (1)$$

where $\mathbf{k}_{\omega}$ and $\mathbf{k}_{2\omega}$ are the wavevectors of the fundamental and SH waves, respectively. $\mathbf{G}_{m,n,l}$ is the 3D reciprocal vector defined as

$$\mathbf{G}_{m,n,l} = m\frac{2\pi}{\Lambda_x}\hat{\mathbf{x}} + n\frac{2\pi}{\Lambda_y}\hat{\mathbf{y}} + l\frac{2\pi}{\Lambda_z}\hat{\mathbf{z}} \quad (2)$$

where $\hat{\mathbf{x}}$, $\hat{\mathbf{y}}$ and $\hat{\mathbf{z}}$ are unit vectors, and m, n and l are integers. The experimental SH patterns with input fundamental wavelengths of 829, 824, 802 and 780 nm are shown in Fig. 3b–e, respectively. The corresponding reciprocal vectors are also labelled, and are calculated according to the emission angles of the SH beams (see Supplementary Sections 3 and 5 for calculation details). The 3D QPM processes can be observed in the SH patterns. As the input fundamental wavelength decreases, the emission angle of the non-collinear SH spot increases because a higher-order reciprocal vector is required to compensate for the phase mismatch. For example, $\mathbf{G}_{\pm1,1,0}$ is involved in the QPM SHG process for input light with a wavelength of 824 nm, while the higher-order reciprocal vector $\mathbf{G}_{\pm3,1,0}$ is required for an input wavelength of 780 nm. Because the QPM wavelengths for the reciprocal vectors with $l = -1$, 0 and 1 are quite close to each other (Supplementary Table 1), the corresponding SH spots form a column, as shown in Fig. 3.

Figure 4a presents the dependence of the collinear SH power on the input fundamental wavelength for the 3D $LiNbO_3$ NPC. The fundamental beam power is kept at 0.6 W. The output SH power reaches a peak at the fundamental wavelength of 829 nm, which indicates that the QPM condition is satisfied. The reciprocal vector involved is $\mathbf{G}_{0,1,0}$. For comparison, we also measured the wavelength dependence of the SH power from the non-engineered area of the $LiNbO_3$ crystal (red curve in Fig. 4a). Clearly, no peak appears in this non-QPM case. At the QPM wavelength of 829 nm, the measured SH power from the engineered area is significantly enhanced compared to that from the non-engineered area (Fig. 4a). Figure 4b depicts the power dependence of the collinear SHG on the input power at the fundamental wavelength of 829 nm. When the fundamental input power is 1.5 W, the directly measured conversion efficiency for collinear SHG reaches $\sim 1.2\times10^{-4}$. The aggregate conversion efficiency of all the collinear and non-collinear SH spots is measured to be 2.3×10^{-4}. Such a conversion efficiency can be further improved by achieving better $\chi^{(2)}$ erasing.

We have experimentally demonstrated a 3D NPC in a $LiNbO_3$ crystal with the femtosecond-laser engineering technique. In addition to the key function of high-efficiency frequency conversion through a 3D QPM mechanism, our work reveals several other unique characteristics. The $LiNbO_3$ crystal is one of the most popular NPC materials, and the demonstrated scheme is easily accessible to researchers working in the field of nonlinear optics and compatible with current technologies in nonlinear optical modulation. The requirements for laser engineering are relatively easy to satisfy, especially along the depth direction, and can be readily extended to a broad range of nonlinear crystals including $LiTaO_3$ and $KTiOPO_4$ crystals. In addition, such a laser engineering method can be feasibly applied to fabricate more complex nonlinear photonic structures for the accurate 3D manipulation of nonlinear optical waves, which have potential applications in nonlinear beam shaping, nonlinear imaging, 3D nonlinear holography and so on[9,10,13,14]. We also note recent progress regarding nonlinear photonic metamaterials[29], which could be a potential alternative avenue for the creation of 3D NPCs.

Note added in proof: During the proofreading stage, we became aware of a work on a 3D NPC in ferroelectric barium calcium titanate[30], providing an alternative means to fabricate 3D NPCs.

Methods

Methods, including statements of data availability and any associated accession codes and references, are available at https://doi.org/10.1038/s41566-018-0240-2.

Received: 18 March 2018; Accepted: 23 July 2018;
Published online: 20 August 2018

References

1. Berger, V. Nonlinear photonic crystals. *Phys. Rev. Lett.* **81**, 4136–4139 (1998).
2. Armstrong, J. A., Bloembergen, N., Ducuing, J. & Pershan, P. S. Interactions between light waves in a nonlinear dielectric. *Phys. Rev.* **127**, 1918–1939 (1962).
3. Fejer, M. M., Magel, G. A., Jundt, D. H. & Byer, R. L. Quasi-phase-matched second harmonic generation: tuning and tolerances. *IEEE J. Quantum Electron.* **28**, 2631–2654 (1992).
4. Yamada, M., Nada, N., Saitoh, M. & Watanabe, K. First-order quasi-phase matched $LiNbO_3$ waveguide periodically poled by applying an external field for efficient blue second-harmonic generation. *Appl. Phys. Lett.* **62**, 435–436 (1993).
5. Broderick, N. G., Ross, G. W., Offerhaus, H. L., Richardson, D. J. & Hanna, D. C. Hexagonally poled lithium niobate: a two-dimensional nonlinear photonic crystal. *Phys. Rev. Lett.* **84**, 4345–4348 (2000).
6. Zhu, S., Zhu, Y. Y. & Ming, N. B. Quasi-phase-matched third-harmonic generation in a quasi-periodic optical superlattice. *Science* **278**, 843–846 (1997).
7. Jin, H. et al. Compact engineering of path-entangled sources from a monolithic quadratic nonlinear photonic crystal. *Phys. Rev. Lett.* **111**, 023603 (2013).
8. Ellenbogen, T., Voloch-Bloch, N., Ganany-Padowicz, A. & Arie, A. Nonlinear generation and manipulation of Airy beams. *Nat. Photon.* **3**, 395–398 (2009).
9. Hong, X. H., Yang, B., Zhang, C., Qin, Y. Q. & Zhu, Y. Y. Nonlinear volume holography for wave-front engineering. *Phys. Rev. Lett.* **113**, 163902 (2014).
10. Bloch, N. V. et al. Twisting light by nonlinear photonic crystals. *Phys. Rev. Lett.* **108**, 233902 (2012).
11. Zhang, Y., Gao, Z. D., Qi, Z., Zhu, S. N. & Ming, N. B. Nonlinear Čerenkov radiation in nonlinear photonic crystal waveguides. *Phys. Rev. Lett.* **100**, 163904 (2008).
12. Trajtenberg-Mills, S., Juwiler, I. & Arie, A. On-axis shaping of second-harmonic beams. *Laser Photon. Rev.* **9**, L40–L44 (2015).
13. Zhang, Y., Wen, J., Zhu, S. N. & Xiao, M. Nonlinear Talbot effect. *Phys. Rev. Lett.* **104**, 183901 (2010).
14. Lu, R. E. et al. Nearly diffraction-free nonlinear imaging of irregularly distributed ferroelectric domains. *Phys. Rev. Lett.* **120**, 067601 (2018).
15. Chen, J. & Chen, X. Phase matching in three-dimensional nonlinear photonic crystals. *Phys. Rev. A* **80**, 013801 (2009).

16. Thomas, J. et al. Quasi phase matching in femtosecond pulse volume structured x-cut lithium niobate. *Laser Photon. Rev.* **7**, L17–L20 (2013).
17. Kroesen, S., Tekce, K., Imbrock, J. & Denz, C. Monolithic fabrication of quasi phase-matched waveguides by femtosecond laser structuring the $\chi^{(2)}$ nonlinearity. *Appl. Phys. Lett.* **107**, 101109 (2015).
18. Rosenman, G., Urenski, P., Agronin, A., Rosenwaks, Y. & Molotskii, M. Submicron ferroelectric domain structures tailored by high-voltage scanning probe microscopy. *Appl. Phys. Lett.* **82**, 103–105 (2003).
19. Yamada, M. & Kishima, K. Fabrication of periodically reversed domain structure for SHG in $LiNbO_3$ by direct electron beam lithography at room temperature. *Electron. Lett.* **27**, 828–829 (1991).
20. Wei, D. et al. Directly generating orbital angular momentum in second-harmonic waves with a spirally poled nonlinear photonic crystal. *Appl. Phys. Lett.* **110**, 261104 (2017).
21. Magel, G. A., Fejer, M. M. & Byer, R. L. Quasi-phase-matched second-harmonic generation of blue light in periodically poled $LiNbO_3$. *Appl. Phys. Lett.* **56**, 108–110 (1990).
22. Xu, T. et al. A naturally grown three-dimensional nonlinear photonic crystal. *Appl. Phys. Lett.* **108**, 051907 (2016).
23. Wu, D. et al. In-channel integration of designable microoptical devices using flat scaffold-supported femtosecond-laser microfabrication for coupling-free optofluidic cell counting. *Light Sci. Appl.* **4**, e228 (2015).
24. Malinauskas, M. et al. Ultrafast laser processing of materials: from science to industry. *Light Sci. Appl.* **5**, e16133 (2016).
25. Ying, C. Y. J. et al. Light-mediated ferroelectric domain engineering and micro-structuring of lithium niobate crystals. *Laser Photon. Rev.* **6**, 526–548 (2012).
26. Boes, A. et al. Direct writing of ferroelectric domains on strontium barium niobate crystals using focused ultraviolet laser light. *Appl. Phys. Lett.* **103**, 142904 (2013).
27. Chen, X. et al. Quasi-phase matching via femtosecond laser-induced domain inversion in lithium niobate waveguides. *Opt. Lett.* **41**, 2410–2413 (2016).
28. Sheng, Y. et al. Three-dimensional ferroelectric domain visualization by Čerenkov-type second harmonic generation. *Opt. Express* **18**, 16539–16545 (2010).
29. Li, G., Zhang, S. & Zentgraf, T. Nonlinear photonic metasurfaces. *Nat. Rev. Mater.* **2**, 17010 (2017).
30. Xu, T. et al. Three-dimensional nonlinear photonic crystal in ferroelectric barium calcium titanate. *Nat. Photon*. https://doi.org/10.1038/s41566-018-0225-1 (2018).

Acknowledgements

This work was supported by the National Key R&D Program of China (2017YFA0303703, 2016YFA0302500 and 2018YFB1105400), the National Natural Science Foundation of China (NSFC) (91636106, 11621091, 11674171, 11627810, 61475149, 61675190 and 51675503) and Youth Innovation Promotion Association CAS (2017495). The authors acknowledge J. Chu, X. Xu, Q. Wang, X. Hong, Y. Liang, S. Li, L. Zhang, Y. Cai, H. Xu, L. Zhang and X. Zhang for help with sample fabrication and characterization.

Author contributions

Y.Z. conceived the idea. D.Z.W., C.W.W., H.J.W., X.P.H., D.W., X.Y.F., Y.L.H. and J.W.L. performed the experiments and numerical simulations under the guidance of Y.Z., D.W., S.N.Z. and M.X. Y.Z. and M.X. supervised the project. All authors contributed to the discussion of experimental results. D.Z.W., Y.Z. and M.X. wrote the manuscript with contributions from all co-authors.

Competing interests

The authors declare no competing interests.

Additional information

Supplementary information is available for this paper at https://doi.org/10.1038/s41566-018-0240-2.

Reprints and permissions information is available at www.nature.com/reprints.

Correspondence and requests for materials should be addressed to Y.Z. or D.W. or S.Z. or M.X.

Publisher's note: Springer Nature remains neutral with regard to jurisdictional claims in published maps and institutional affiliations.

Methods

Sample parameters. The laser-engineered 3D $LiNbO_3$ NPC crystal has a tetragonal structure. The laser-modified unit cell was designed to be cylindrical, as shown in Fig. 1b. The periodic lengths between cells are 3 μm (*x*), 3 μm (*y*) and 11 μm (*z*), and the repeated structure layers are 30 (*x*), 30 (*y*) and 4 (*z*), respectively. The duty cycles in the *x*, *y* and *z* directions are 50, 50 and 54.5%, respectively.

Laser engineering of the $LiNbO_3$ crystal. A typical femtosecond-laser writing system was used to produce microstructures in the $LiNbO_3$ crystals. The light source was a mode-locked Ti:sapphire laser system with a regenerative amplifier (Legend Elite-1K-HE Coherent) working at a wavelength of 800 nm. The pulse width was 104 fs and the repetition rate 1 kHz. The laser beam passed through a beam expander and was then focused into the $LiNbO_3$ crystal by an objective (×50, numerical aperture = 0.8). The sample position was precisely controlled by a nanopositioning stage (Physik Instrument, E545) with a resolution of 1 nm and a moving range of 200 μm (*x*) × 200 μm (*y*) × 200 μm (*z*). The laser writing process can be observed by a charge-coupled-device (CCD) camera in real time. We used a scanning strategy with a compensation technology to improve the desired uniformity for each layered structure. The writing laser energies were 100, 150, 180 and 200 nJ from the top to bottom layers with scanning speeds of 100, 85, 70 and 55 μm s^{-1}, respectively. The size of the focal spot inside the sample was ~1.2 μm in the transverse direction and ~5–10 μm in the axis direction (depending on the fabrication depth). See Supplementary Section 4 for details of the fabrication and optimization processes.

Experimental scheme for demonstrating 3D QPM SHG processes. The fundamental beam was a Ti:sapphire femtosecond laser (Chameleon, Coherent) with a tunable wavelength ranging from 690 to 1,050 nm. The polarization of the input laser beam was along the *z* direction so that the largest nonlinear coefficient d_{33} of the $LiNbO_3$ crystal could be utilized. After focusing by a 50 mm lens, the fundamental beam was incident into the sample. The focal waist was ~40 μm, comparable to the thickness of the 3D NPC structure. The output far-field SH patterns were projected onto a screen and recorded by a camera. A power meter was used to measure the collinear QPM SH power. See Supplementary Section 8 for details of the experimental set-up.

Data availability. The data that support the plots within this paper and other findings of this study are available from the corresponding authors upon reasonable request.